World Journal of Advanced Research and Reviews
eISSN: 2581-9615 CODEN (USA): WJARAI
Cross Ref DOI: 10.30574/wjarr
Journal homepage: https://wjarr.com/

(RESEARCH ARTICLE)

Check for updates

Structural characterization and magnetic Behaviour of nickel oxide nanoparticles synthesized using greener route

Ramalakshmi Mariappan [1,*] and Ranesh Jagadev Shakkthivel [2]

[1] *Department of Applied Sciences and Pharmacy, University of Technology and Applied Sciences – Muscat, Sultanate of Oman.*
[2] *Department of Mechanical Engineering, Chennai Institute of Technology, Sarathy Nagar, Kundrathur, Chennai, India.*

World Journal of Advanced Research and Reviews, 2025, 26(02), 4489–4496

Publication history: Received on 20 April 2025; revised on 28 May 2025; accepted on 31 May 2025

Article DOI: https://doi.org/10.30574/wjarr.2025.26.2.2121

Abstract

NiO nanoparticles were synthesized by a two-step approach using a small amount of ionic liquid [Bmim][TfO] was found to be an effective stabilizing agent. The thermal, structural, morphological and magnetic characterization of the resulting samples were investigated by means of Thermogravimetry (TGA), X-ray powder diffraction (XRD), Fourier transform infrared spectroscopy (FT-IR), Field emission scanning electron microscopy (FE-SEM), Transmission electron microscopy (TEM) and Vibrating sample magnetometer (VSM) analysis and the results indicate that the hexagonal β-$Ni(OH)_2$ upon calcination at 400ºC to form cubic NiO nanoparticles and are superparamagnetic in nature. We believe that this method can be developed into a general way to synthesize other metal oxide nanoparticles on a large scale.

Keywords: Nanostructures; Heat treatment; Precipitation; Electron microscopy; Fourier transform infrared spectroscopy; Magnetic properties

1. Introduction

Nickel hydroxide $Ni(OH)_2$, as one of the most important transition metal hydroxides, has received increasing attention due to its wide applications, such as electric vehicles, portable electronics, power tools, positive electrode active material, etc [1]. NiO also equally receives more attention in the mentioned applications. There are two polymorphs of Ni $(OH)_2$, which are designated as α–$Ni(OH)_2$ and β-$Ni(OH)_2$ forms. Among these the hexagonal β- $Ni(OH)_2$ phase is brucite-like and well-oriented $Ni(OH)_2$ layers are perfectly stacked along the C-axis with an interlamellar distance of 4.60°A [2-5]. Recently, the synthesis of $Ni(OH)_2$ nanocrystals including nanoparticles, nanotubes and nanoribbons, nanosheets, hollow microspheres, and flower-like structures have been reported [6].

Nickel oxide (NiO) has rhombohedral or cubic structure demonstrated a variety of practical applications such as electrochromic material for smart windows [7,8], gas sensing [9], photovoltaics [10,11], catalysis [12,13], light-emitting devices [14], electrochemical capacitors [15,16] and degradation of various dyes, through photocatalytic processes [17,18]. NiO exhibits excellent magnetic [19], optical and electrochemical properties [20] and it can be used as p-type semiconducting layer [21]. Particular attention has been devoted to the synthesis of various shapes of nanosized NiO materials by various routes such as thermal decomposition, sol-gel, microemulsion, hydrothermal and precipitation methods [22-25]. Ionic liquids (ILs) seem to be ideal for the stabilization of nanoparticles. The intrinsic ionic charge, high polarity, high dielectric constant and supramolecular network of ILs provide an electrostatic protection according to the DLVO theory in the form of protective shell for the nanoparticles, so that no extra stabilizing agents are needed [26-28]. In our group, we have been synthesized various metal oxide nanoparticles using [Bmim][TfO] IL [29,30]. Hence, an attempt has been made for the synthesis of NiO, a potentially application-oriented material for the magnetic and

* Corresponding author: Ramalakshmi Mariappana.

biomedical field applications. For the first time, the method of ionic liquid-assisted metal oxide precipitation route has been adopted, particularly [Bmim][TfO] IL is used for the NiO synthesis and their structural dependent magnetic characteristics are explained.

2. Experimental Details

2.1. Synthesis of Nickel Oxide (NiO) Nanoparticles

Nickel nitrate hexahydrate ($(Ni(NO_3)_2.6H_2O$) and ethanol were purchased from E-Merck, India and 1-n-butyl-3-methylimidazolium trifluromethane sulfonate ionic liquid [Bmim][TfO] IL was purchased from E-Merck, Germany and used as received. All the solutions were made using deionized water. Approximately 0.1M solution of nickel (II) nitrate hexahydrate solution was mixed with the 0.25% [Bmim][TfO] IL solution in dropwise manner with stirring and the reaction mixture was maintained at pH 11 using NaOH and stirring was continued for an hour. Immediately after the addition of NaOH solution the pale green colour precipitate of $Ni(OH)_2$ nanoparticles were formed. The precursor (nickel hydroxide) residue was washed with water and ethanol for several times and dried in vacuum.

The effect of [Bmim][TfO] IL concentration at 0.5% and 0.75% on the nickel oxide formation was also studied. The as-synthesized samples were interrogated for TGA analysis to confirm the NiO nanoparticle formation and further the samples were calcined at 400°C for 3 hours in air and kept in vacuum for further analysis. The gained black nickel oxide nanoparticles were analyzed for their chemical, structural, morphological and their magnetic properties.

2.2. Characterization

The thermal behaviour of $Ni(OH)_2$ and calcined at 400°C was investigated under nitrogen atmosphere using TGA-Q50 V 20.6 Build 31 thermogravimetric analyzer at a heating rate of 10°C/min. The phase purity of the products were examined on a Panlytical X'Pert PRO Diffractometer with Cu Kα radiation (λ = 1.5405 °A). A fourier transform infrared spectra was taken on a SHIMADZU 8400-S. The size and morphology of the products were determined by field emission scanning electron microscopy (FE-SEM: HITACHI S-4800) and transmission electron microscopy (TEM: HITACHI H-7500, operating at an accelerating voltage of 200kV). Magnetization (M-H curve) measurements were made out using vibrating sample magnetometer (VSM: Lakeshore -7404).

3. Results and Discussion

3.1. TGA Studies

Nickel oxide (NiO) nanoparticles were synthesized through calcination of β-$Ni(OH)_2$ nanoparticles precipitated from 0.75% [Bmim][TfO] IL medium. The $Ni(OH)_2$ nanoparticles were calcined at 400°C and their respective TGA spectra are presented in Figure 1. The TGA curves exhibit dehydration and decomposition in a four-step as it is observed from the weight loss. The first stage weight loss is related to the evaporation of the adsorbed and intercalated water molecules associated with the $Ni(OH)_2$. $X_{ads}H_2O$ deposit.

$$\mathbf{Ni(OH)_2.X_{ads}H_2O \longrightarrow Ni(OH)_2 + XH_2O}$$

The consequent three stage weight losses upto 501°C are could be due to the decomposition of β-$Ni(OH)_2$ and ionic liquid covered on the nanoparticles. It is possible to estimate the water content in the as-prepared β-$Ni(OH)_2$. The quantity of water present in the nanoparticle plays an important role in the crystal structure and their electrochemical and catalytic properties [31].

The conversion of β-$Ni(OH)_2$ into NiO occurs between 270°C and 350°C which is very well correlated with the reported values [4,32,33]. In fact, at this range the loss is associated with water elimination produced by the dehydroxylation of hydroxide layers.

$$\mathbf{Ni(OH)_2 \longrightarrow NiO + H_2O}$$

The last three stage weight loss in the TG curve is about 19.3% (Fig.1 as-synthesized), which is in good agreement with the theoretical weight loss value (19.4%) caused by the decomposition of β-$Ni(OH)_2$ [34-37]. The TGA result proves that the as-prepared sample is β-$Ni(OH)_2$. An insignificant weight loss in the temperature range of 350-460°C could be observed in the TGA curve may attribute to the decomposition of IL covered on the nanoparticles.

The pyrolysis of the precursor was complete before the calcination temperature of 400°C. In order to ascertain the above fact, we have subjected the as-prepared samples calcined at 400°C for 3 hours and the respective thermogram is presented in Figure 1, a reduced weight loss for the removal of chemisorbed water can be seen except a negligible weight loss occurred for the IL, which exhibits the possibility of pure form of NiO formation at this temperature.

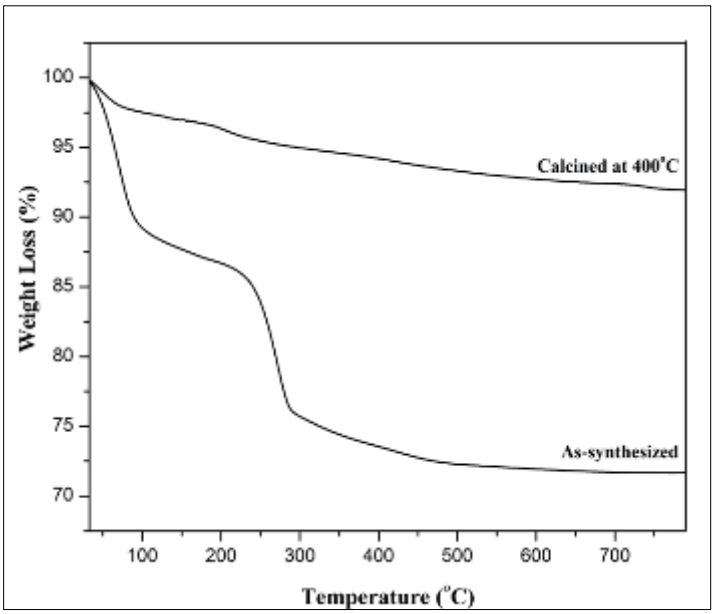

Figure 1 TGA Curves of as-synthesized β-Ni(OH)$_2$ nanoparticles and calcined at 400°C using 0.75% [Bmim][TfO] IL

3.2. XRD Studies

The as-synthesized β-Ni(OH)$_2$ nanocrystals in various concentration of ionic liquid (0.25%, 0.5% and 0.75%) were calcined at 400°C. The purity and phase of the above samples were characterized by X-ray powder diffraction and their resulting patterns are presented in Figures 2a & b. The reflection peaks of the XRD patterns for the as-prepared Ni(OH)$_2$ sample could be indexed to the single phase β-form of nickel hydroxide with the hexagonal structure (JCPDS : 14-0117) [34]. With the presence of no impurity peaks suggest that the high purity of β-Ni(OH)$_2$ samples. The average crystallite size of the β-Ni(OH)$_2$ samples estimated by the Scherrer's equation are 45, 37 and 30 nm for the samples synthesized in the 0.25%, 0.5% and 0.75% of IL medium respectively.

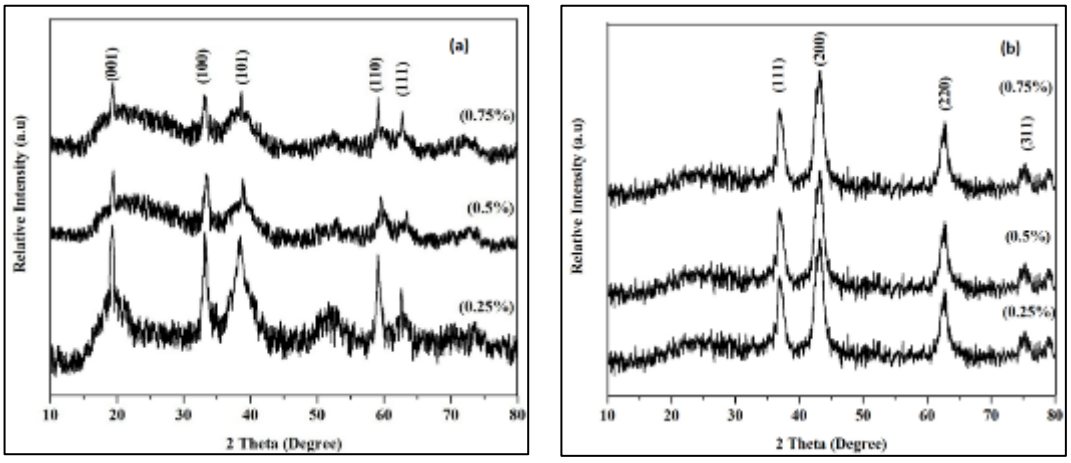

(a) (b)

Figure 2 XRD patterns of (a) as-synthesized β-Ni(OH)$_2$ nanoparticles and (b) calcined at 400°C using different [Bmim][TfO] IL concentrations

The Figure 2b depicts the XRD patterns of the 400°C calcined β-Ni(OH)$_2$ nanoparticles. The identification patterns observed at different 2θ angles can be correlated with the pure cubic phase of NiO (Fm3m, JCPDS: 78-0429). The

crystallite sizes were estimated to be in the range of 60-41 nm [35,37]. Increasing the IL concentration, the particles become smaller, and while increasing the calcination temperature the size of the nanoparticles are increased. The appealing behaviour of formation of small crystallites can be correlated with the anionic moieties in the [Bmim][TfO] IL exhibit good electrostatic interaction with nickel cation lead to the formation of reduced particle size. The IL extend its uniqueness in avoiding the aggregation of nanoparticles and acts as template for the synthesis.

3.3. FT-IR Studies

The FT-IR spectral studies were performed for the as-prepared samples using different concentration of IL (0.25%, 0.5% and 0.75%) and for the samples calcined at 400°C and the resulting spectra are illustrated in Figures 3a &b. The FT-IR bands are corroborated with the TGA and XRD results for the presence and absence of water adsorbed on the particle's surface in the as-prepared and calcined at 400°C samples respectively. The as-prepared $Ni(OH)_2$ nanoparticle's FT-IR spectra verified that the prepared $Ni(OH)_2$ samples can be categorized for β-form of $Ni(OH)_2$ due to the existence of a narrow and strong band at 3640 cm^{-1} relating to the ν-OH stretching vibration which indicates the –OH group in a free configuration. The band at 520 cm^{-1} appears strongly, which can be ascribed to the hydroxyl groups lattice vibrations δ(-OH), and also the band at around 460 cm^{-1} is resulting from the Ni-O lattice vibration [32,33,36,38-40]. Conversely, the disappearance of band at 3640 cm^{-1} in the 400°C calcined sample can be seen, which indirectly indicates the formation of NiO nanoparticles from $Ni(OH)_2$ form. Further, the peaks for Ni-O bond lattice vibration at 460 cm^{-1}, the sharp vibration peak at around 3400 cm^{-1} for –OH vibration and for bending vibrations of water molecule at 1670 cm^{-1} are noted. The presence of prominent peak at 1120 cm^{-1} is attributed to the C-N stretching mode of IL. Scanty amount of IL presence on the particle surface is unavoidable and the IL has very strong electrostatic force.

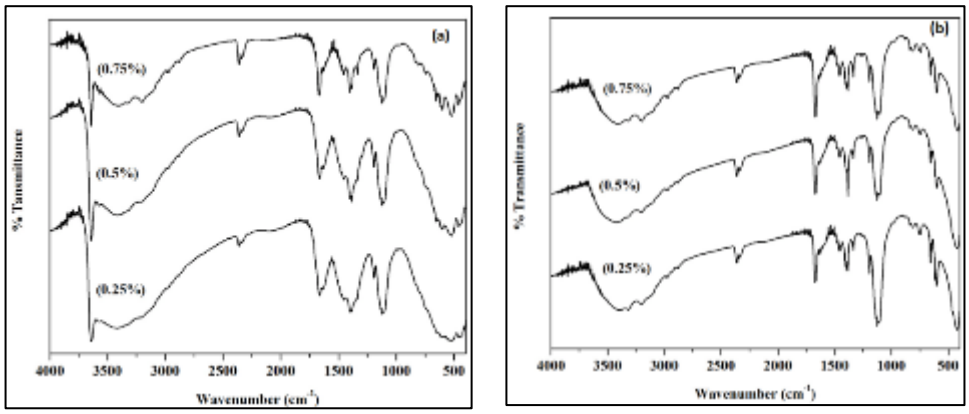

(a) (b)

Figure 3 FT-IR spectra of (a) as-synthesized β-$Ni(OH)_2$ nanoparticles and (b) calcined at 400°C using different [Bmim][TfO] IL concentrations

3.4. FE-SEM Studies

In order to obtain the insight information about the surface morphology and particle size of the $Ni(OH)_2$ and NiO samples synthesized in various concentration of IL, FE-SEM analysis were performed and micrographs are presented Figures 4. The formation of nano β-$Ni(OH)_2$ particles are clearly visible and the particles are in the size range of 50 to 500 nm. Bigger size particles are aggregated crystals of rock-like morphology in the as-synthesized $Ni(OH)_2$ particles in 0.25% IL. As the calcination temperature increases, the aggregated particle size is increased two-fold. The calcined β-$Ni(OH)_2$ particles at 400°C, the aggregation of NiO nanoparticles become sheet-like structure. The NiO architectures are built by the precipitation process of β-$Ni(OH)_2$ decomposition at 400°C for 3 hours. The 400°C calcined samples composed of sheet like particles with a size range of 400-750 nm, 90-410 nm and 60-180 nm for the samples synthesized from 0.25%, 05% and 0.75% IL respectively [41]. Increasing the ionic liquid concentration in the synthesis medium, particles aggregation is prevented notably, however, with increase in calcination temperature the particles are agglomerated become bigger in size, these can be observed from the FE-SEM micrographs.

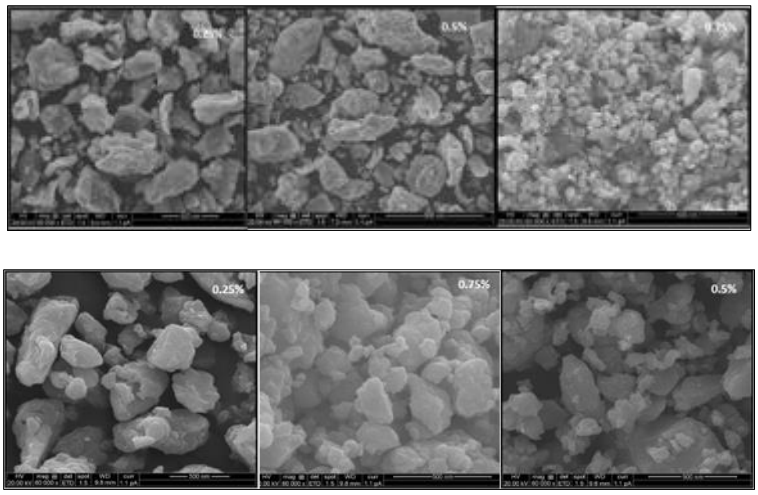

Figure 4 FE-SEM micrographs of as-synthesized β-$Ni(OH)_2$ nanoparticles and calcined at 400°C using different [Bmim][TfO] IL concentrations

3.5. TEM Studies

The TEM analysis of the sample provides the significant information about the size, morphology and their state of agglomeration. The TEM and SAED pattern of NiO nanoparticles synthesized from 0.75% [Bmim][TfO] IL (calcined at 400°C) are presented in Figure 5. It can be seen from the TEM figure that the particles are in sheet-like morphology, but not homogeneously dispersed. The inset figure shows the corresponding SAED pattern of the NiO particles, all the diffraction rings can be indexed to the cubic phase of NiO [42]. The TEM and SAED patterns are confirmed the NiO nanoparticles are FCC structure, which is well consistent with XRD results.

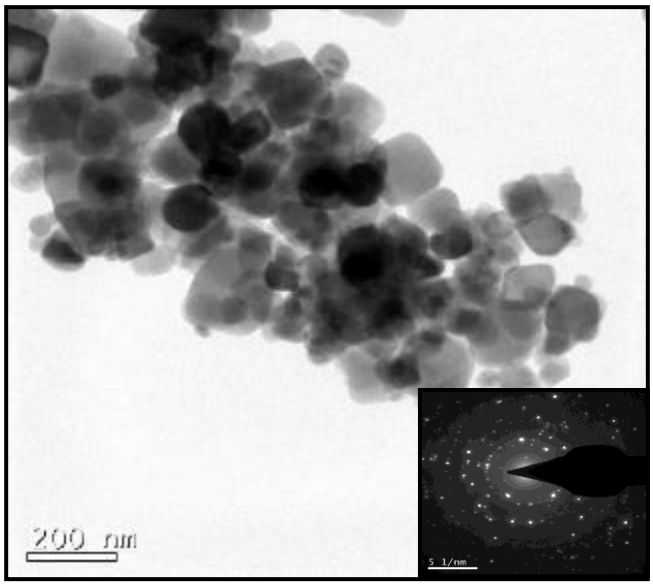

Figure 5 TEM image NiO nanoparticles synthesized using 0.75% [Bmim][TfO] IL and calcined at 400°C (Inset SAED pattern)

3.6. VSM Studies

The magnetic properties of the synthesized NiO nanoparticles in 0.25%, 0.5% and 0.75% IL calcined at 400°C were evaluated and their resulting M-H curves are presented in Figure 6. For NiO, anti-ferromagnetism is observed by many authors and loop shift is most likely linked to the exchange bias between the surface layer and the inner core in the coupled systems like Co/NiO, Co/CoO, etc. With the decrease of crystallite size, the surface area to volume ratio increases which leads to increase in the fraction of atoms present on or near the surface and number of defects and missing bonds. Consequently, the co-ordination number gets reduced which in turn causes modification in the exchange

interaction between the surface atoms. Origin of such size dependent magnetization behaviour is still not very well understood [43]. In the present study, at room temperature, no magnetic saturation is found for all the samples, which can be accounted by the strong particle size dependent characteristics behaviour. The linear magnetization curve with the magnetic field can be seen with a lattice splitting of loop except for the 0.75% IL sample, which exhibit superparamagnetism, which is influenced by the finite size and surface effects. However, there is still some debate regarding the origin of such effects going on [42,44].

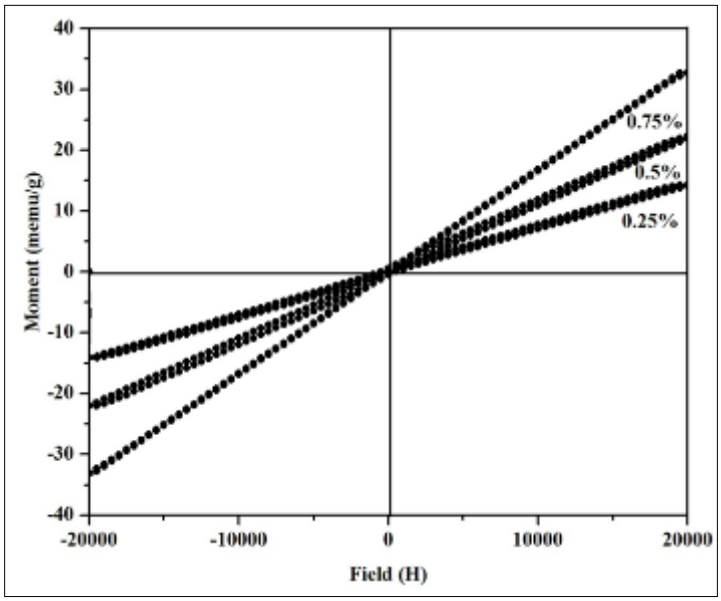

Figure 6 M-H Curves of NiO nanoparticles synthesized using different [Bmim][TfO] IL concentrations

4. Conclusion

The [Bmim][TfO] IL was exploited for the synthesis of NiO magnetic nanoparticles. The formation of NiO nanoparticles was confirmed by the TGA analysis, the decomposition of $Ni(OH)_2$ occurs beyond 300°C. The as-synthesized samples were indexed to β form of $Ni(OH)_2$ and the XRD peak broadening with increasing the IL concentration for the as-prepared samples was found as the particle size reduction. However, the 400°C calcined sample illustrates that the pure cubic phase of NiO form. The FT-IR spectral results corroborated with the XRD and TGA results that the appearance of 3640 cm^{-1} band in the as-synthesized samples relates to the ν-OH stretching vibration of $Ni(OH)_2$ which was not observed in the 400°C calcined samples, indicates the formation of NiO. The size of $Ni(OH)_2$ nanoparticles is reduced with increasing the IL concentration (120nm to 25nm) and the rock like morphology is transferred into the sheet like structure on calcination as observed from FE-SEM and TEM micrographs. The XRD and SAED pattern reveals the NiO nanoparticles is polycrystalline cubic structure. A linear magnetization curve with the magnetic field was observed for all the synthesized NiO samples and exhibit superparamagnetic character, where the particles synthesized in 0.25% and 0.5% IL show a negligible loop opening. However, no splitting of magnetization in the positive and negative applied field for the samples synthesized in 0.75% IL was noted due to the finite size effect. Thus, the concentrated IL support for the NiO nanoparticle growth through the highly structured hydrogen bonded network, further, the nanoparticles exhibit the finite size effect, which is useful for the biomedical, electronics and specialized applications.

Compliance with ethical standards

Disclosure of conflict of interest

No conflict of interest to be disclosed.

References

[1] S.R. Ovshinsky, M.A. Fetcenko, J. Ross, Science 260 (1993) 176.

[2] C. Coudun, J.F. Hochepied, J. Phys. Chem. B 109 (2005) 6069.

[3] X.Y. Wang, H. Luo, P.V. Parkhutik, A.C. Millan, E. Matveeva, J. Power Sources 115 (2003) 153.

[4] L.X. Yang, Y.J. Zhu, H. Tong, Z.H. Liang, L. Li, L. Zhang, J. Solid State Chem. 180 (2007) 2095.

[5] T.N. Ramesh, P.V. Kamath, J. Power Sources 156 (2006) 655.

[6] X.C. Song, X. Wang, Z.A. Yang, Y.F- Zheng, Mater. Lett. 65 (2011) 2348.

[7] G.A. Niklasson, C.G. Grangvist, J. Mater. Chem. 17 (2007) 127.

[8] M.S. Wu, C.–H. Yang, Appl. Phys. Lett. 91 (2007) 033109.

[9] K.I. Arshak, L.M. Cavanagh, I. Gaidan, E.G. Moore, S.A. Clifford, IEEE Sens. J. 7 (2007) 925.

[10] S.S. Kim, K.W. Park, J.H. Yum, Y.E. Sung, Sol. Energy Mater. Sol. Cells 90 (2006) 283.

[11] J. He, H. Lindstrom, A. Hagfeldt, S.E. Lindquist, J. Phys. Chem. B 103 (1999) 8940.

[12] J. Li, R. Yan, B. Xiao, D.T. Liang, D.H. Lee, Energy Fuels 22 (2008) 16. H.A. Mahmoud, A.A.A. Ali, T.T. Ali , B.M.A. Zied, Sohag J. Sci. 2025, 10(1), 34.

[13] H.A. Mahmoud, A.A.A. Ali, T.T. Ali , B.M.A. Zied, Sohag J. Sci. 2025, 10(1), 34.

[14] Y.Y. Xi, D. Li, A.B. Djurisic, A.M.C. Ng, W.K. Chan, H.L. Tam, K.W. Cheah, Appl. Phys. Lett. 92 (2008) 113505.

[15] D.D. Zhao, M.W. Xu, W.J. Zhou, J. Zhang, H.L. Li, Electrochim. Acta 53 (2008) 2699.

[16] Y.Y. Xi, D. Li, A.B. Djurisic, M.H. Xie, K.Y.K. Man, W.K. Chan, H.L. Tam, K.W.Chan, Electrochem. Solid State Lett. 11 (2008) D56.

[17] S.D. Khairnar, V.S. Shrivastava, Journal of Taibah University for Science, 13 (2019) 1108.

[18] N.A. Khan, K. Saeed, I. Khan, T. Gul, M. Sadiq, A. Uddin, I. Zekker, Applied Water Science, 12 (2022) 131.

[19] M.M. Natile, A. Glisenti, Chem. Mater 15(2003) 2502.

[20] X. Wang, J. Song, L. Gao, J. Jin, H. Zheng, Z. Zhang, Nanotechnology 16 (2005) 37.

[21] H. Sato, T. Minami, S. Takata, T. Yamada, Thin solid films 236 (1993) 27.

[22] C.S. Carney, C.J. Gump, A.W. Weimer, Mater. Sci. Engg. A 431 (2006) 13.

[23] Y. Wu, Y.H. He, T.H. Wu, T. Chen, W.Z. Weng, H.L. Wan, Mater. Lett. 61 (2007) 3174.

[24] D.Y. Han. H.Y. Yang, C.B. Shen, X. Zhou, F.H. Wang, Powder Technol. 147 (2004) 113.

[25] M.A. Lopez-Quintela, Curr. Opin. Colloids Int. Sci. 8 (2003) 137.

[26] J. Dupont, J. Braz. Chem. Soc. 15 (2004) 341.

[27] E.J.W. Verwey, J.T.G. Overbeek, Theory of the stability of Lyophobic Colloids, 2nd Ed. Dover Publications, Mineola, New York, (1999).

[28] B.W. Ninham, Adv. Colloid Interface Sci. 83 (1999) 1.

[29] M. Ramalakshmi, M. Sundrarajan, Mater. Res. Bull. 48 (2) (2013) 618.

[30] M. Ramalakshmi, P. Shakkthivel, M. Sundrarajan, S.M. Chen Mater. Res. Bull. 48 (8) (2013) 2758.

[31] Q. Song, Z. Tang, H. Guo, S.L.I. Chan, J. Power Sour. 12 (2002) 428.

[32] G.S. Illia, M. Jobbagy, A.E. Regazzoni, M.A. Blesa, Chem. Mater. 11 (1999) 3140.

[33] P. Baraldi, G. Davolio, G. Fabbri, T. Manfredini, Mater. Chem. Phys. 21 (1989) 479.

[34] B. Zhao, X.K. Ke, J. H. Bao, C.L. Wang, L. Dong, Y.W. Chen, et.al., J. Phys. Chem. C 113 (2009) 14440.

[35] M.S. Niasari, N. Mir, F. Davar, Polyhedron 28 (2009) 1111.

[36] M. Aghazadeh, A.N. Golikand, M. Ghaemi, Int. J. Hyd. Energy 36 (2011) 8674.

[37] L. Fang, L. Jing, S. Jun. Z. Zhao, Mater. Chem. Phys. 113 (2009) 18.

[38] R. Acharya, T. Subbiah, S. Anand, R.P. Das, J. Power Sour. 109 (2002) 494.

[39] P.V. Kamath, G.N. Subbanna, J. Appl. Electrochem. 22 (1992) 478.

[40] P. Baraldi, G. Davolio, Mater. Chem. Phys. 21 (1989) 143.

[41] Z. Zhu, N. Wei, H. Liu, Z. He, Advanced Powder Tech. 22 (2011) 422.

[42] M.Y. Ge, L.Y. Han, U. Wiedald, X.B. Xu, C. Wang, K. Kuepper, P. Ziemann, J.Z. Jiang, Nanotechnology 21 (2010) 425702.

[43] S. Thota, J. Kumar, J. Phys. Chem. Solids 68 (2007) 1951.

[44] N.M. Carneiro, W.C. Nunes, R.P. Borges, M. Godinho, L.E.F. –Outon, W.A.A. Macedo, I.O. Mazali, J. Phys. Chem. C 114 (2010) 18773.